

Material Science Experiments on the Atlas Facility

R.K. Keinigs , W.L. Atchison, W.E. Anderson , R.R. Bartsch , R.J. Faehl ,
E.C Flower-Maudlin , J.E. Hammerberg , D.B Holtkamp , M.E. Jones , G. Kyrala ,
I.R. Lindemuth , D.M. Oro , J.V. Parker , D.L. Preston, R.E. Reinovsky , G. Rodriquez ,
D.W. Scudder , P.T. Sheehey , J.S. Shlachter , J. Stokes , A.J. Taylor , D.L. Tonks ,
P.J. Turchi , E. Chandler *

Los Alamos National Laboratory
Los Alamos, New Mexico 87545

Abstract

Three material properties experiments that are to be performed on the Atlas pulsed power facility are described; friction at sliding metal interfaces, spallation and damage in convergent geometry, and plastic flow at high strain and high strain rate. Construction of this facility has been completed and experiments in high energy density hydrodynamics and material dynamics will begin in 2001.

I. THE ATLAS FACILITY

Figure 1 shows the physical configuration of the facility: a 23 MJ capacitor bank is housed in 12 separate Marx tanks surrounding a central target chamber that houses the experiments [1]. Each tank contains four Marx modules having four capacitors charged up to +/- 60 kV and two railgap switches. When the switches are triggered at maximum voltage, the 96 modules erect in parallel to 240 kV. A set of 24 tapered, oil-insulated vertical tri-plate transmission lines carry current to a diameter of 2.5 m, at which point a transition section couples the current to a radial power flow channel (PFC). The PFC delivers the current to a cylindrical metal shell, aka, "liner" load, and the $j \times B$ force on the liner causes it to implode.

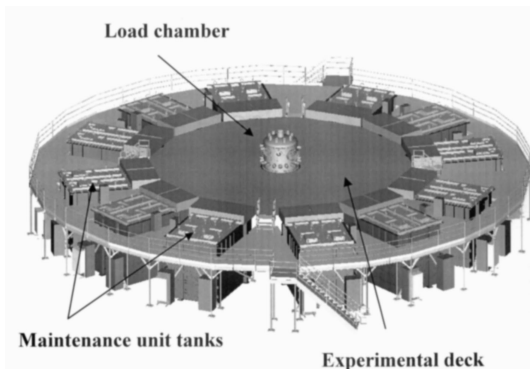


Figure 1. Schematic of the Atlas facility, showing capacitor tanks, transmission lines, and the central target chamber that houses the experiment.

* Lawrence Livermore National Laboratory

When Atlas is discharged at maximum voltage, 32 MA of current are produced in a quarter cycle time of approximately 5 μ s. At a radius of 5 cm this current corresponds to a magnetic pressure of 90 kB. This large pressure can impart on the order of 1.5 to 2 megajoules of kinetic energy to a relatively massive 45-gram aluminum liner (1.6mm thick, 4 cm in height). A typical liner is shown in Figure 2.

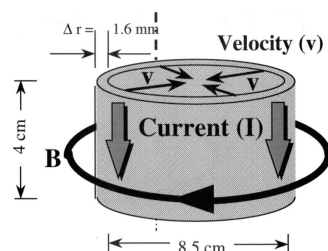


Figure 2. Liner load for an Atlas experiment.

Corresponding implosion velocities as high as 1.4 cm/ μ s can be generated. The liner can be used either as a cylindrical flyer plate for target-based experiments, or, the liner itself can be interrogated to study instability growth of machined perturbations. Based upon B-dot probe data collected on the Pegasus pulsed power facility (Atlas's predecessor) it is anticipated that a 5 cm radius liner can be imploded to a radius of 1 cm with an error in the cylindrical symmetry of less than 0.1 % [2]. It is this especially high degree of symmetry, coupled with the high energy and convergence that make an Atlas a unique experimental venue for investigating dynamic material properties in extreme, high energy density environments.

II. FRICTION

Leonardo DaVinci studied friction during the early 16th century, demonstrating that the "normal" frictional force between two surfaces is independent of the contact area and is proportional to the normal, applied force. The purpose of the Atlas friction experiments is to

Report Documentation Page			Form Approved OMB No. 0704-0188					
<p>Public reporting burden for the collection of information is estimated to average 1 hour per response, including the time for reviewing instructions, searching existing data sources, gathering and maintaining the data needed, and completing and reviewing the collection of information. Send comments regarding this burden estimate or any other aspect of this collection of information, including suggestions for reducing this burden, to Washington Headquarters Services, Directorate for Information Operations and Reports, 1215 Jefferson Davis Highway, Suite 1204, Arlington VA 22202-4302. Respondents should be aware that notwithstanding any other provision of law, no person shall be subject to a penalty for failing to comply with a collection of information if it does not display a currently valid OMB control number.</p>								
1. REPORT DATE JUN 2001	2. REPORT TYPE N/A	3. DATES COVERED -						
4. TITLE AND SUBTITLE Material Science Experiments on the Atlas Facility			5a. CONTRACT NUMBER					
			5b. GRANT NUMBER					
			5c. PROGRAM ELEMENT NUMBER					
6. AUTHOR(S)			5d. PROJECT NUMBER					
			5e. TASK NUMBER					
			5f. WORK UNIT NUMBER					
7. PERFORMING ORGANIZATION NAME(S) AND ADDRESS(ES) Los Alamos National Laboratory Los Alamos, New Mexico 87545		8. PERFORMING ORGANIZATION REPORT NUMBER						
9. SPONSORING/MONITORING AGENCY NAME(S) AND ADDRESS(ES)			10. SPONSOR/MONITOR'S ACRONYM(S)					
			11. SPONSOR/MONITOR'S REPORT NUMBER(S)					
12. DISTRIBUTION/AVAILABILITY STATEMENT Approved for public release, distribution unlimited								
13. SUPPLEMENTARY NOTES See also ADM002371. 2013 IEEE Pulsed Power Conference, Digest of Technical Papers 1976-2013, and Abstracts of the 2013 IEEE International Conference on Plasma Science. IEEE International Pulsed Power Conference (19th). Held in San Francisco, CA on 16-21 June 2013. U.S. Government or Federal Purpose Rights License.								
14. ABSTRACT Three material properties experiments that are to be performed on the Atlas pulsed power facility are described; friction at sliding metal interfaces, spallation and damage in convergent geometry, and plastic flow at high strain and high strain rate. Construction of this facility has been completed and experiments in high energy density hydrodynamics and material dynamics will begin in 2001.								
15. SUBJECT TERMS								
16. SECURITY CLASSIFICATION OF: <table border="1"> <tr> <td>a. REPORT unclassified</td> <td>b. ABSTRACT unclassified</td> <td>c. THIS PAGE unclassified</td> </tr> </table>			a. REPORT unclassified	b. ABSTRACT unclassified	c. THIS PAGE unclassified	17. LIMITATION OF ABSTRACT SAR	18. NUMBER OF PAGES 5	19a. NAME OF RESPONSIBLE PERSON
a. REPORT unclassified	b. ABSTRACT unclassified	c. THIS PAGE unclassified						

measure the “tangential” force between two metal interfaces that are moving at high relative velocity. (Note that throughout the friction section of this article, velocity refers to the relative velocity of the two materials in contact.)

Theories of interfacial dynamics indicate that the dissipation mechanisms involved in sliding friction are related to the plastic properties of the weaker material. These include dislocation and phonon dynamics, microstructural changes, and crystalline melting. Figure 3 shows schematically the velocity regimes in which these different mechanisms are thought to dominate. In this figure the tangential force is scaled by the material shear modulus and the velocity is scaled by the transverse sound speed. Typical engineering experiments provide data only in very low velocity regimes, $v/c_t < 0.01$. Pegasus experiments were able to reach regimes, $v/c_t \sim 0.05$. Atlas driven liners will allow making measurements in even higher regimes, $v/c_t \sim 0.1$, in which the tangential force is predicted to decrease as $(v/c_t)^\beta$, where β is to be experimentally determined.

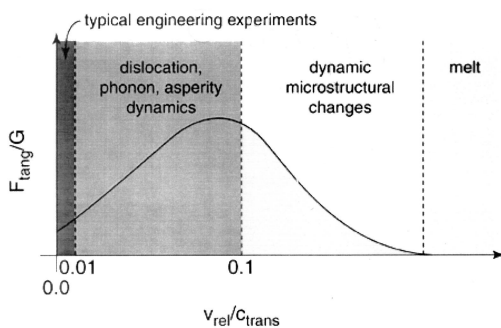


Figure 3. Schematic diagram showing the tangential frictional force as a function of relative sliding velocity.

Atlas friction experiments will be conducted using a similar methodology to friction experiments fielded on Pegasus, which were performed in order to demonstrate proof-of-principle of the technique. In both the Pegasus and Atlas experiments, high velocity sliding is produced by using an imploding liner to generate shocks in a target comprised of two adjacent, dissimilar materials. The different shock and particle speeds in the two materials result in a velocity shear being produced at the contact interface of the materials. This relative velocity can be increased by having the liner impact the target at higher velocity. This can be done in a variety of ways: thinning the liner, thus reducing its mass, discharging the bank at a higher voltage, or changing the starting liner radius.

The optimal approach has not yet been determined. The time-varying tangential force between the materials is inferred by embedding very thin lead wires in the materials, perpendicular to the contact interface, and radiographing the wires’ distortions for several times during the shock evolution. From the radiographic images the bending of the wires can then be measured and compared to the corresponding positions of the Lagrangian mesh lines from simulations employing different fitting parameters for the constitutive frictional force, e.g., the parameter, β , for the force law at high velocities (see Figure 3). Figure 4a shows a static radiograph of a target from one of three Pegasus friction experiments. The view is along the cylindrical axis of the target. The white area depicted is a vacuum region in the center of the aluminum (grey) / tantalum (black) target. The Pb wires are clearly shown. Aluminum and tantalum will also be employed in the first Atlas experiments, but the target geometry will be different, having the tantalum and aluminum parts “stacked” axially.

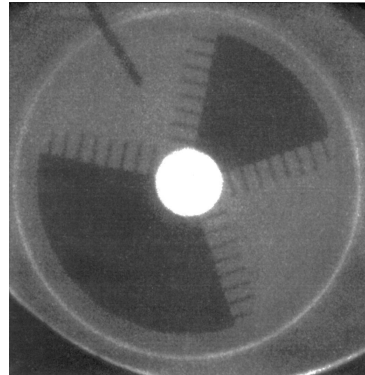


Figure 4a. Static radiograph of a “wedge” tantalum and aluminum target showing initial placement of the lead tracer wires.

The radiograph shown in Figure 4b was taken approximately 4.6 μ s after liner impact with the target, and indicates how the wires have been deformed as a result of the interfacial motion between the two materials. Note that the vacuum region has closed as aluminum, which has the higher shock and material velocity, has moved into this region. The “light” layer in Fig. 4b is a region of lower density aluminum. This represents a region where the material spalled as a result of intersecting release waves. Though not seen in the radiograph, post-shot metallurgical analyses of the recovered target also show distinct spalled and damaged regions in the tantalum.

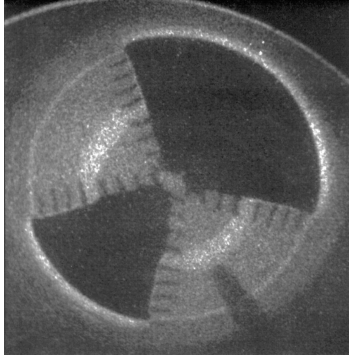


Figure 4b. Dynamic radiograph taken after the shock has moved material into the central, originally vacated, target region. Bending of the wires is clearly visible.

III. SPALL AND MATERIAL DAMAGE

Quantifying spall and evaluating damage in convergent geometry is a second materials experiment to be performed on Atlas. First explained qualitatively by Hopkinson in 1945, spall occurs as the result of intersecting release waves putting a material into a stress state of tension. If the tensile stress exceeds a threshold value, commonly referred to as the “spall strength”, then voids will begin to nucleate and coalesce, providing an initiation path to damage. Figure 5 is a schematic of the spallation process in planar geometry [4].

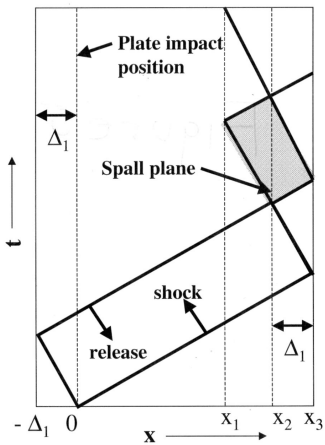


Figure 5. Distance-time plot showing intersecting release waves creating a region of tension in the target (shaded area).

In this depiction of a planar spall experiment, an impactor having a thickness, Δ_1 , moves from left to right, impacting the target at $t=0$, $x=0$. Impact is followed by two shocks; one propagating forward into the target, and one propagating backward into the impactor. The shocks release

from the free surfaces at x_3 and $-\Delta_1$ respectively. The release waves (often referred to as rarefactions) intersect at x_2 , thus putting the material into a state of negative pressure. A simple x-t analysis, for a symmetric impact (identical materials), show that the spall plane will be located a distance, Δ_1 , inside the free surface of the target.

Determining the spall strength of a material is a difficult undertaking, often requiring “sneaking up” on the phenomenon by doing a number of experiments at different pressures, then micrographically examining the spalled target to determine at what pressure spall is initiated. Attempting to quantifying spall without detailed post-processing of recovered targets, Cochran and Banner [5] defined two parameters, the pullback velocity, $v_p = v_A - v_B$, and a parameter, $R = v_C/v_A$, both of which can be obtained by using interferometry (VISAR) to measure the “free surface” velocity of an impacted target [5]. These parameters indicate the spall strength and degree of damage, respectively. Figure 6 shows a typical velocity profile of this surface for two cases, spall and no spall. In the case on no spall the surface velocity increases upon breakout of the shock, and then decreases back to zero. In the case of internal spall of the target, one or more oscillations in the surface velocity are seen. These oscillations are due to internal wave reflections from the spalled region of the material returning to the free surface and providing an additional “kick”.

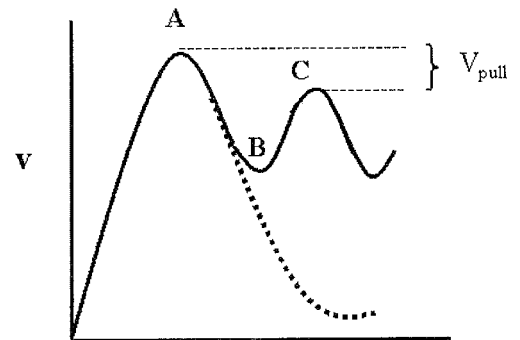


Figure 6. Schematic of a VISAR signal from the free surface velocity of an impacted target. For no internal spall the velocity monotonically decreases after peak (dotted line). For internal spall oscillations will occur (solid line).

The damage parameter is not discussed in this paper. The pullback velocity is approximately related to the spall strength, Σ , via the equation,

$$\Sigma = \frac{1}{2} \rho_0 c v_p, \quad (1)$$

where c defines a velocity somewhere between the longitudinal and bulk sound speeds in the material. VISAR will be employed on Atlas to measure the pullback velocity, and compare this signal with that obtained in planar gas gun experiments. However, in the Atlas experiments there are anticipated complications because of both the convergence and the fact that the magnetic drive is operational long after initial spall occurs. Continuous drive means that damage could be evolving during the entire time of the experiment. (This is actually one of the principal reasons for doing these experiments.) However, this damage evolution also will make it difficult to correlate void distributions from post-processing of the recovered target material with the VISAR signals. To help with this task, future experiments will include multi-frame radiography in order to follow the evolution of the spalled material. Simulations in one dimension have been performed to determine the dimensions of the liner and target, and the bank voltage required in order to produce the desired shock amplitude and profile. The first set of experiments will be to generate a "Taylor-like" profile with an amplitude at the inner target surface of approximately 50 -70 kB. The simulated shock at different positions within the target is shown in Figure 7.

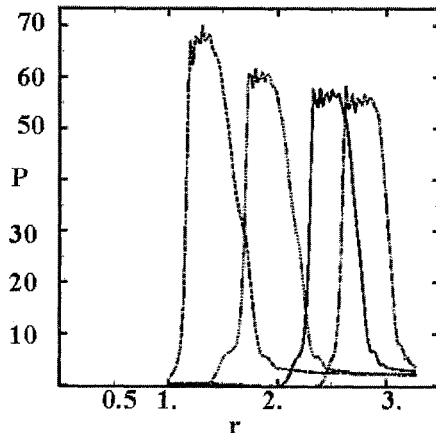


Figure 7. Pressure profiles (in kbars) within the target taken at four different positions. Impact occurs at a radius of 3.3 cm. The inner surface of the target is located 1.0 cm from the axis.

IV. STRENGTH AT HIGH STRAIN AND HIGH STRAIN RATE

The third materials dynamics experiment to be performed on Atlas pertains to the strength of metals undergoing large deformations at very high strain rates. The strength, or the plastic flow stress of a material, σ , can depend upon several variables; the amount of material strain (ε), the

strain rate ($\dot{\varepsilon}$) and temperature; even the deformation history. Many models for the flow stress have been concocted for incorporation into hydrodynamic codes, and many experimental techniques for measuring stress-strain behavior have been developed. However, the models are typically empirically based, with the experiments providing data for generating fitting parameters for the models. An example of one such model is the Johnson-Cook model, which is expressed as [4]:

$$\sigma_{JC} = \sigma_y (1 + B\varepsilon^P) \left[1 - \left(\frac{T}{T_m} \right)^n \right] x \left(1 + C \ln\left(\frac{\dot{\varepsilon}}{\dot{\varepsilon}_0}\right) \right) \quad (2)$$

In this equation σ_y defines the yield strength at zero temperature and T_m defines the melt temperature. The first bracketed term in this equation represents strain hardening and the second term represents thermal softening. The last term represents strain-rate hardening. The fitting parameters, $\{B, P, \alpha, n, C\}$, for low strain rates ($< 1 \text{ sec}^{-1}$) are typically obtained from quasistatic pressure experiments, for higher strain rates, ranging from $10 - 10^4 \text{ sec}^{-1}$, split Hopkinson bar pressure experiments are commonly used. Plate impactors and laser driven flyers can produce extremely high strain rates, but are limited to low % strain. The experimental strain / strain-rate phase space for these and other standard techniques is shown in Figure 8. Phase space regimes accessible by pulsed power facilities such as Pegasus and Atlas are also shown. The high liner velocity attainable with Atlas permits reaching strain rates $\sim 10^6 \text{ sec}^{-1}$, while the high convergence ratio admits strains $\sim 200\%$.

Two approaches will be tried in investigating strength using the Atlas bank; neither uses a target, but instead interrogates only the liner as it is imploded. One approach has been fielded on Pegasus, and that is to use infrared pyrometry to measure the plastic heating arising from work done on the inside surface of the liner as it implodes. The temperature rise from plastic heating is given in Equation (3),

$$\Delta T = \frac{\beta}{\rho C_V} \int_0^\varepsilon d\varepsilon' \sigma(\varepsilon', \dot{\varepsilon}', T, \dots), \quad (3)$$

where C_V defines the heat capacity, ρ is the material density, and β is a conversion factor ~ 0.9 . By measuring the temperature rise and differentiating with respect to strain, one obtains a direct measurement of the flow stress at this

surface. This stress can then be compared to numerical calculations for ΔT using different strength models.

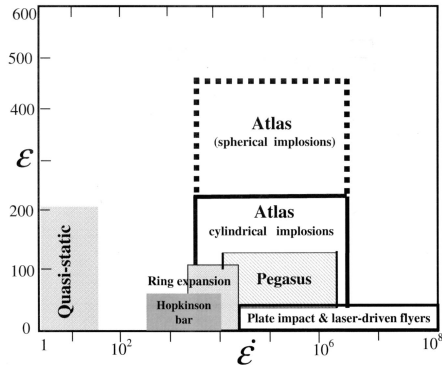


Figure 8. Strain / strain rate regimes for different experimental techniques used in determining the plastic flow stress. Y-axis is strain (%), the X-axis is strain rate (sec^{-1}).

The second approach to be tried in investigating strength will be to use multi-frame radiography to monitor the growth rate of machined perturbations in multi-material liners. The liner geometry is designed so that it is unstable to Rayleigh-Taylor (RT) instabilities. Unlike RT instabilities in a fluid for which all wavelengths are unstable, RT instabilities in strong media depend upon wavelength. For sufficiently short wavelengths the material strength can suppress growth of perturbations. A great deal of theoretical and experimental work on the influence of strength on the stability of explosively driven flyer plates has been performed by our Russian colleagues [7]. Figure 9 shows one such liner configuration that has been suggested by V.N. Mokhov [8]. A composite liner comprised of an upper metal layer, a middle working fluid, and a lower metal layer, is driven radially inward by magnetic pressure on the upper metal. The interface separating the light fluid from the lower metal layer has prescribed, machined perturbation. With the fluid being less dense than the metal, this perturbed interface is will be unstable, and the perturbations will grow as the liner implodes. Growth rates inferred from radiographs taken at different times during the liner implosion can then be compared to calculated growth rates from simulations using different strength models.

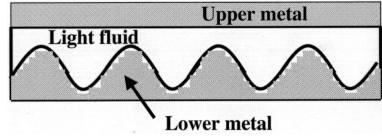


Figure 9. Proposed multi-material liner with imposed perturbations. JxB force is on upper metal layer.

V. CONCLUSIONS AND ISSUES

Three material science experiments that will be fielded on the Atlas pulsed power facility have been described. Each experiment takes advantage of the convergent geometry offered by Atlas, and the high currents that can be used to drive metal liners to high velocities. Diagnostics is of paramount importance in successfully fielding these experiments. The VISAR diagnostic yields precise position of moving surfaces (liner and / or target). Multi-point and line VISAR are desirable. Radiography is critical to all three experiments, and both improved resolution (higher dose) and multi-frame capability is being actively developed.

VI. REFERENCES

- [1] H.A. Davis, R.K. Keinigs, et.al., "The Atlas High-Energy Density Project", *Jpn. J. Appl. Phys.*, vol. 40 (2001) pp. 930-934
- [2] J. S. Stokes, private communication
- [3] J.E. Hammerberg, G.A. Kyrala, D.M. Oro, R.D. Fulton, et.al., "A Pegasus Dynamic Liner Friction Experiment", in *Shock Compression of Condensed Matter – 1999*, M.D. Furnish, L.C. Chhabildas, and R.S. Hixson, eds., 2000 American Inst. of Physics 1-56396-923, p.1217
- [4] M.A. Meyers, *Dynamic Behavior of Materials*, John Wiley & Sons, Inc. New York, New York, 1994
- [5] S. Cochran and D. Banner, *J. of Appl. Phys.* 48, #7 (1977), p.2729
- [6] L. Barker and J. Hollenbach, "Interferometry Technique for Measuring the Dynamical Mechanical Properties of Materials", *Rev. Scient. Instr.* 36, (1965), p. 1617
- [7] S.M.Bakhrakh, O.B. Drennov, N.P Kovalev, A.I. Lebedev, et. al. "Hydrodynamic Instability in Strong Media" (unpublished review of VNIIEF publications, LLNL-VNIEFF Report)
- [8] V.N. Mokhov, private communication